ELSEVIER

Chemical Engineering Science 61 (2006) 823–834

Chemical Engineering Science

www.elsevier.com/locate/ces

Adhesion of solid particles to gas bubbles. Part 1: Modelling

Florin Omota[a], Alexandre C. Dimian[a,*], Alfred Bliek[b]

[a]*Department of Chemical Engineering, University of Amsterdam, Nieuwe Achtergracht 166, 1018 WV, Amsterdam, The Netherlands*
[b]*Faculty of Science and Technology, Twente University of Technology, P.O. box 217, 7500 AE, Enschede, The Netherlands*

Received 10 March 2005; received in revised form 15 May 2005; accepted 5 July 2005
Available online 30 August 2005

Abstract

Particle-to-bubble adhesion is important in the areas of anti-foaming, in flotation processes and in multiphase slurry reactors. In the present work we particularly address the latter. The behaviour of fine catalyst particles adhering to gas bubbles in aqueous media is governed by the surface hydrophobicity. This adhesion on its turn influences the G–L mass transfer, bubble coalescence and the particle agglomeration. Existing models for the quantitative description of adhesion of particle to a G–L interface usually assume nonporous, spherical particles with a smooth surface and a well-defined contact angle. As catalyst particles are normally highly porous, have a rough surface, and an irregular shape, we developed a generalised model describing the adhesion of particles to a gas bubble based on maximum adhesive and cohesive forces as the main parameters. This model describes adhesion of: (i) a single spherical particle, (ii) a monolayer of particles, and (iii) a particle agglomerate. The cohesive forces between particles play a key role. For small cohesive forces, the particles can either adhere as a single particle or as a monolayer, while stronger cohesive forces allow multilayer adhesion or adhesion of particle clusters via one or few particles.

Keywords: Modelling; Particle; Adhesion; Agglomeration; Bubble; Flotation

1. Introduction

Three-phase reactors are the workhorses of chemical industry. The presence of solid catalyst particles may influence reactor hydrodynamics through their impact on the apparent viscosity and liquid density, but moreover by its impact on the bubble coalescence and G–L mass transfer. Typical examples of chemical processes carried out via such three-phase reactors are selective hydrogenation and oxidation. G–L mass transfer enhancement was observed when fine solid particles are present at the G–L interface (Alper et al., 1980; Alper and Öztürk, 1986; Wimmers and Fortuin, 1988; Tinge and Drinkenburg, 1992, 1995; Beenackers and van Swaaij, 1993; Joly-Vuillemin et al., 1996; van der Zon et al., 1999). The adhesion of catalyst particles to gas bubbles plays a key role in the mass transfer mechanism for the oxidation of organic compounds (Lee and Tsao, 1972; Alper et al., 1980; Lavelle and McMonagle, 2001) or hydrogenation reactions in aqueous media (Wimmers et al., 1988; Dietrich et al., 1992; Vinke et al., 1992; van der Zon et al., 1999). However, the nature of this influence is still subject of debate. Different mechanisms have been proposed to explain G–L mass transfer enhancement: (i) a reduced coalescence rate when adhering solid particle cover gas bubbles and the specific surface area a_L increases (Lindner et al., 1988); (ii) so-called "shuttle effect" that consist in gas transfer from G–L interface to bulk liquid through adsorbing particles (Alper et al., 1980; Vinke et al., 1992); (iii) large particles can create turbulence effect on G–L interface increasing both, k_L and a_L; (iv) large particles can divide or stretch the bubbles at Weber numbers higher than 3, increasing a_L.

Vinke et al. (1991a) and van der Zon et al. (1999) showed that small hydrophobic particles may adhere to bubbles in aqueous slurries, while hydrophilic particles do not. Vinke et al. (1992) introduced the concept of *bubble coverage* defined as the fraction of bubble surface covered with adhering

* Corresponding author. Tel.: +31 20 525 6034; fax: +31 20 525 5604.
E-mail address: alexd@science.uva.nl (A.C. Dimian).

0009-2509/$ - see front matter © 2005 Elsevier Ltd. All rights reserved.
doi:10.1016/j.ces.2005.07.005

particles. This concept is useful when a monolayer of particles covers the lower part of a bubble. Based on the equilibrium of all forces involved, the bubble coverage may be calculated.

The higher G–L mass transfer observed when catalyst particles adhere to the G–L interface may be described in terms of an enhancement factor, defined as the ratio of gas-absorption mass transfer in the presence of solid particles and gas-absorption mass transfer without particles, under similar hydrodynamic conditions (Wimmers et al., 1988; Vinke et al., 1992, 1993; Joly-Vuillemin et al., 1996; van der Zon et al., 1999; Dagaonkar et al., 2003). The models proposed by these authors for the estimation of G–L mass transfer in slurry reactors, correlates the enhancement factor with the solid concentration in the slurry and the surface fraction of a bubble covered by particles.

Clearly, particle to bubble adhesion is affected by particle agglomeration. Vinke et al. (1991a) observed for Pd/Al_2O_3 and $Pd/BaSO_4$ catalysts that particle-to-particle cohesion dominates the particle-to-bubble adhesion due to the formation of large clusters, which are no longer able to adhere to hydrogen bubbles in water. In case of Pd/C catalyst particles, the particle-to-bubble adhesion dominates the particle-to-particle cohesion resulting in full bubble coverage. van der Zon et al. (2001) demonstrated that particle agglomeration significantly affects adhesion, in particular under stagnant conditions and for high G–L superficial tension. Despite this evident effect of agglomeration, the cohesive forces between particles are not usually accounted for in quantitative models describing particle-to-bubble adhesion.

Vinke et al. (1992) investigated the effect of liquid velocity on the particle-to-bubble adhesion. The experiments have shown that Pd/C and Rh/C particles are still able to adhere to the gas bubble for superficial liquid velocities exceeding the terminal rise velocity of a bubble in a liquid. Under these hydrodynamic conditions, the adhesion of particles to hydrogen bubble in aqueous solutions was described by a Langmuir-type adhesion isotherm. This hypothesis suggests that the fraction of bubble surface covered with particles under nonstagnant hydrodynamic conditions is proportional to that under stagnant conditions.

The objective of this work is to develop a novel model describing the adhesion of particles to a gas bubble under stagnant conditions, thereby explicitly taking cohesive forces into account, and allowing a superior prediction of the behaviour of hydrophobic particles subject to competitive adhesion and agglomeration. For small cohesive forces, particles adhere to a bubble individually or as a monolayer as shown in Fig. 1a,b. For cohesive forces exceeding a certain limit, a second layer can be attached to the first one (Fig. 1c). When the cohesion forces are higher than the adhesion forces, the particles agglomerate in rigid clusters that can adhere to a gas bubble through a single or only few particles (Fig. 1d). Thus, the strength of cohesion forces affects the fraction of bubble coverage as well as the maximum weight of particles carried by a bubble. The model developed here could also be useful in the flotation practice.

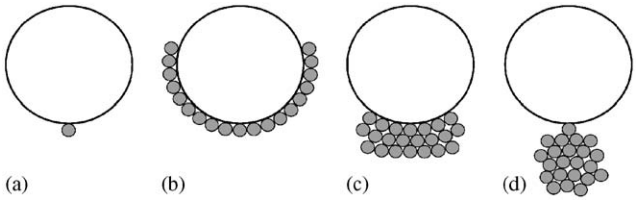

Fig. 1. Schematic view of particles adhering to a gas bubble: (a) single particle, (b) monolayer, (c) multilayer, and (d) cluster of particles suspended through a single particle.

2. Model development

A theoretical framework will be developed here to describe adhesion of solid particles to gas bubbles under stagnant conditions, based on the equilibrium of capillary forces, gravity forces and pressure forces. The following four cases can be distinguished:

- Adhesion of a single particle to a gas bubble
- Monolayer adhesion for negligible cohesive forces
- Multilayer adhesion for moderate cohesive forces
- Adhesion of a cluster of particles for strong cohesive forces

The model will initially refer to the simple case of:

- Spherical particles with identical size and physical properties
- Homogeneous and smooth particle surface and therefore a well defined contact angle
- Particle density higher than the liquid density
- Spherical bubbles

Finally, the model will be generalised to the case of porous particles with irregular shape and heterogeneous surface, due to the interest of exploiting particle-to-bubble adhesion in the case of heterogeneously catalysed reactions. A shortcoming of the model based on the contact angle is its applicability to spherical particles.

The major problem of modelling particle-to-bubble adhesion is the fractal-like structure of catalyst particles. Three-phase contact angle can be easily and accurately measured on clean, homogeneous and smooth surfaces. In all other cases, the contact angle ranges between two extreme values; the advancing and receding contact angle depending on the measurement technique which makes this parameter even harder to obtain (Ortiz-Arroyo et al., 2003). The contact angle of powdered non-porous particles can be measured by Washburn method, based on the capillary rise technique. However, this method gives only advancing contact angles rather than equilibrium angles. As result of porosity

and roughness of the surface, the appearing contact angle measured by Washburn method is smaller than in the case of smooth solid surface (Chibowski and Perea-Carpio, 2002). Different investigators use different methods of calculating contact angles from the heat of immersion but the methods reported in the literature used gross assumptions, which may be the source of inaccuracy in determining water contact angles (Malandrini et al., 1997; Yan et al., 2000). Even accurate measurements would be available by one or other techniques, the adhesion behaviour might be also influenced by the particle architecture: shape, porosity and roughness, not only by the three-phase contact angle.

The adhesion behaviour depends on the adhesive forces. Therefore, instead of calculating the adhesion forces of a spherical particle from the contact angle, we use the adhesion force as a model parameter. Both two approaches, based on the contact angle or maximum adhesion force, allow us to correlate the structure of particle aggregate adhering to a gas bubble with the particle–particle cohesive and particle–bubble adhesive forces.

3. Adhesion of a single particle to a gas bubble

3.1. Force balance

Solid particles can adhere to a gas bubble if the capillary forces are strong enough to compensate the apparent weight of particles and the gas pressure. Under static conditions, the equation describing the equilibrium forces of a single particle attached at the gas–liquid interface (Fig. 2) is given below:

$$F_g + F_p - F_b - F_c = 0 \tag{1}$$

where F_g is the gravitational force of a single particle, F_p is the force resulting from the capillary pressure inside the gas bubble, F_b is the buoyancy force, and F_c is the capillary force. Fig. 2a shows a solid particle adhering to a free G–L interface, corresponding to a bubble having an infinitely large radius. Fig. 2b shows a solid particle of radius R_p, adhering to a gas bubble of finite radius R_b. The corresponding force denoted by F_p is positive in the case (a), and negative in the case (b). Shultze (1984) studied the adhesion forces on spherical bubbles fixed at a plane solid surface and spherical particles at the flat fluid interface, as shown in Fig. 2a. When we limit ourselves to the case (b), i.e., small particles and small bubbles, the following force balance equations apply:

$$F_g = \frac{4\pi R_p^3 \rho_S g}{3}, \tag{2}$$

$$F_p = \frac{2\gamma_{LG}}{R_b}\,\pi R_p^2 \sin^2\varphi, \tag{3}$$

$$F_b = \frac{\pi R_p^3}{3}(1+\cos\varphi)^2(2-\cos\varphi)\rho_L g, \tag{4}$$

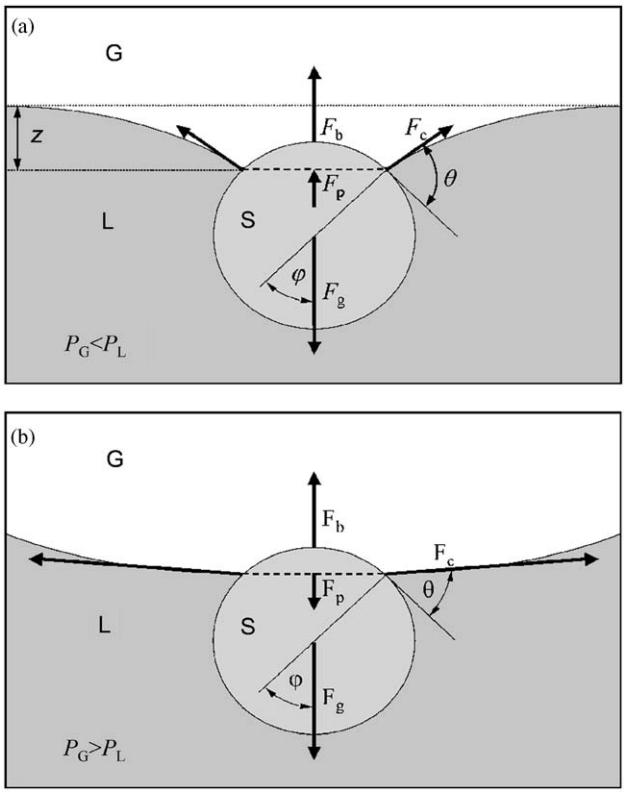

Fig. 2. Representation of the forces acting on a particle: (a) adhering to a flat gas–liquid interface—the hydrostatic pressure has positive effect on adhesion, and (b) to a spherical bubble—the bubble overpressure reduces the adhesion strength.

$$F_c = 2\pi R_p \gamma_{LG} \sin\varphi \sin(\theta - \varphi). \tag{5}$$

For nonporous particles, ρ_S refers to the solid density. For porous particles with a three-phase contact angle $\theta \leqslant 90°$, ρ_S is the density of particles with liquid-filled pores. When $\theta > 90°$, ρ_S stands for the density of particles having the pores filled with gas due to capillary forces. Obviously, highly porous particles may have a lower density than liquid and these particles float at the liquid surface.

For a varying penetration angle φ, the forces defined by Eqs. (2)–(5) may not be in equilibrium, according to Eq. (1). The detachment force F_d is defined as the net force acting downward:

$$F_d = F_g + F_p - F_b - F_c. \tag{6}$$

When $F_d > 0$, the particle moves away from the bubble, the penetration angle φ decreases and ultimately the particle detaches from the G–L interface. $F_d < 0$ corresponds to a particle forced to enter in the gas bubble, and the equilibrium is reached for $F_d = 0$. For negative values of F_d it is more convenient to use the adhesion force of a particle to a bubble, defined as $F_{\text{adh}} = -F_d$.

Fielden et al. (1996) measured the external force necessary to detach a particle adhering to a gas bubble. This force

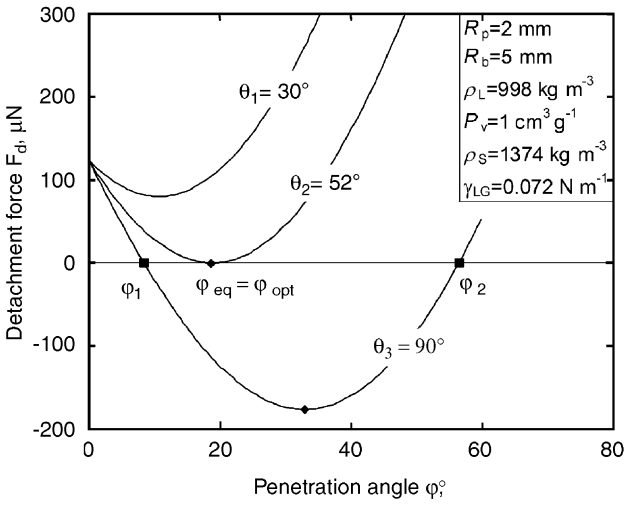

Fig. 3. Influence of the contact angle θ and penetration angle φ on the detachment force F_d of a spherical particle adhering to a gas bubble.

was called normalised detachment force (F_{det}/R_p) and has positive values while F_d considered in this work is negative. The adhesion forces of small spherical particles were also measured by atomic force microscopy by Preuss and Butt (1998). They defined the adhesion force as the force necessary to pull off the particle adhering to bubble. We used in this work the same definition, but including the impact of the apparent particle weight and bubble pressure.

3.2. Influence of particle hydrophobicity

Fig. 3 shows the influence of the penetration angle φ and particle surface hydrophobicity expressed as three-phase contact angle θ on its adhesion properties. For $\varphi = 0$, the particle is completely immersed in the liquid. As the particle density is considered higher than the liquid density, the resulting force F_d is positive. At the interface, the detachment forces F_d are: (a) always positive for low three-phase contact angles, (b) positive except for a single equilibrium position, and (c) negative on a certain interval of the penetration angle, with two equilibrium positions at φ_1 and φ_2.

In case (a), hydrophilic particles larger than a critical size do not adhere to the air bubble, as the detachment force F_d is positive for any penetration angle φ. For larger contact angles the capillary forces increase too, as results from Eq. (5). The detachment force approaches zero in the case (b). The forces acting on the adhering particle are in equilibrium only for a penetration angle φ_{eq}. This is an unstable position, as any perturbation will lead to particle detachment. In the case (c) of more hydrophobic particles compared with the case (b), there are two equilibrium positions corresponding to the penetration angles φ_1 and φ_2. If $\varphi < \varphi_1$, the detachment force is positive $F_d > 0$, the particle moves downward and sinks in the liquid. If $\varphi_1 < \varphi < \varphi_2$, the detachment force is negative, the particle is attracted to the bubble until it reaches the other equilibrium position. For $\varphi > \varphi_2$, the detachment force is positive and the particle moves back at lower penetration angle, φ_2. Thus, the equilibrium positions are unstable at φ_1 and stable at φ_2. The potential energy has a local maximum at φ_1 and a local minimum at φ_2. The existence of a minimum energy at φ_2 demonstrates the stability of particle–bubble aggregate.

3.3. Maximum adhesion force

The detachment force versus the penetration angle always shows a minimum (Fig. 3). For a negative value of F_d an external force is required for particle detachment. The maximum adhesion force defined as $F_{\text{adh,max}} = \max(-F_d)$ characterises the capability of a single particle to remain attached to gas bubble under external forces. For positive values of F_d, the particle does not adhere to the gas bubble and the particle–bubble interactions are repulsive. The penetration angle corresponding to the maximum adhesion force can be found by differentiating F_d with regard to the angle φ, as given by the next equation:

$$\sin(\theta - 2\varphi_{\text{opt}}) = \frac{R_p}{R_b}\sin(2\varphi_{\text{opt}}) + \frac{\rho_L g R_p^2}{2\gamma_{LG}}\sin^3\varphi_{\text{opt}}. \quad (7)$$

Fig. 3 illustrates the behaviour of relatively large particles ($R_p = 2\,\text{mm}$). Smaller particles ($R_p < 0.1\,\text{mm}$) have negligible weight compared to the capillary forces. Therefore, the penetration angle corresponding to the unstable position φ_1 is close to 0 while the penetration angle corresponding to the stable position φ_2 is close to θ. The parabolic form of the detachment force leads to the conclusion that the minimum of the penetration angle is around of $\theta/2$. A better approximation of the penetration angle φ_{opt} derived from Eq. (7) is given below:

$$\varphi^*_{\text{opt}} = \frac{\theta}{2} - \frac{R_p}{2R_b}\sin\theta - \frac{\rho_L g R_p^2}{4\gamma_{LG}}\sin^3\frac{\theta}{2}. \quad (8)$$

In the case of particles smaller than 100 μm, the capillary force exceeds the other forces, except when the contact angle θ is zero or near zero. Thus, the capillary force may approximate the maximum adhesion force of a small spherical particle:

$$F^*_{\text{adh,max}} = 2\pi\gamma_{LG}R_p\sin^2\frac{\theta}{2}. \quad (9)$$

The maximum adhesion force of spherical particles depends on the three-phase contact angle. However, the influence of three-phase contact angle on the adhesion behaviour depends on the particle shape. Adhesion of a nonspherical particle to a gas bubble is better characterised by the maximum adhesion force than by the three-phase contact angle only.

4. Particle aggregates adhering to a gas bubble through a single particle

For large cohesive forces between particles agglomerates may form, and aggregates rather than single particles may adhere to a gas bubble. Let us analyse first the case of an aggregate suspended to a gas bubble through a single particle. All other particles are completely immersed in the liquid and the buoyancy force of these particles becomes

$$F_b^s = \frac{4\pi R_p^3}{3}\rho_L g. \tag{10}$$

The apparent gravity force of a particle completely immersed in liquid and having liquid filled pores will be further denoted by

$$F_a = F_g - F_b^s. \tag{11}$$

The detachment force for an agglomeration of N particles is presented below:

$$F_d^N = (F_g + F_p - F_b - F_c) + (N-1)F_a. \tag{12}$$

The total number of particle N_T attached to a bubble through a single particle has a maximum value that can be found from Eq. (12) using $F_{\text{adh,max}}$:

$$N_T = 1 + \frac{F_{\text{adh,max}}}{F_a}. \tag{13}$$

According to Eq. (13), the maximum adhesion force $F_{\text{adh,max}}$ of a single particle can be found from the maximum number of particles $N_{\max}$ in the cluster. The number of particles N_T is a measure of the adhesion strength, but comparing to $F_{\text{adh,max}}$ it is a dimensionless parameter.

Fig. 4 shows the maximum number of porous silica particles suspended to a gas bubble, for a varying contact angle and the solid particle size. Both $F_{\text{adh,max}}$ and N_T increases by increasing the contact angle. For small particles, the bubble size does not have a significant influence on the adhesion behaviour expressed in terms of N_T, while for large particles, an increase in the bubble size results in a stronger particle-to-bubble adhesion.

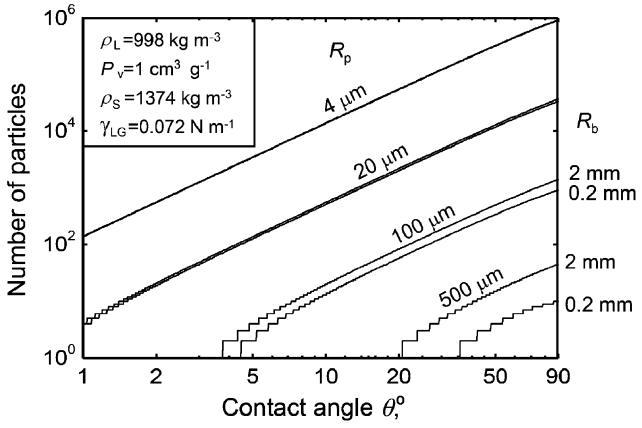

Fig. 4. Influence of three-phase contact angle θ, particle radius R_p and bubble radius R_b on the number of particles in a cluster adhering to a gas bubble through a single particle. Note that the number of particles is a discrete variable.

5. Monolayer adhesion

We will consider a gas bubble of uniform radius R_b, and identical particles with the radius R_p each of them adhering to the bubble. All the particles placed at the same height will be referred as a *level*. The centre of particles belonging to a level describes a circle. The shortest length between two points belonging to consecutive circles will be further referred as the distance between two levels, d_i. We remark that d_i is not the distance between the planes containing the circles.

In vertical cross-section, Fig. 5 shows three particles placed on the levels $i-1$, i and $i+1$. Any particle at level i forms an angle α_i with the bubble of centre C and the symmetry axis S. The distance between the centres of two particles in direct contact is $2R_p$. The distance d_i between two consecutive levels can be smaller because of the overlap of consecutive levels (see Fig. 6). The angle $\Delta\alpha = \alpha_{i+1} - \alpha_i$ corresponding to any two adjacent levels can be calculated from

$$\sin\frac{\Delta\alpha}{2} = \frac{d_i}{2(R_p + R_b)}. \tag{14}$$

The particles are identical and the packing of particles is homogeneous. Thus, the distance d_i and the angle $\Delta\alpha$ between two levels are considered irrespective of the level position i. The angle α_i becomes

$$\alpha_i = i\Delta\alpha, \quad i > 0. \tag{15}$$

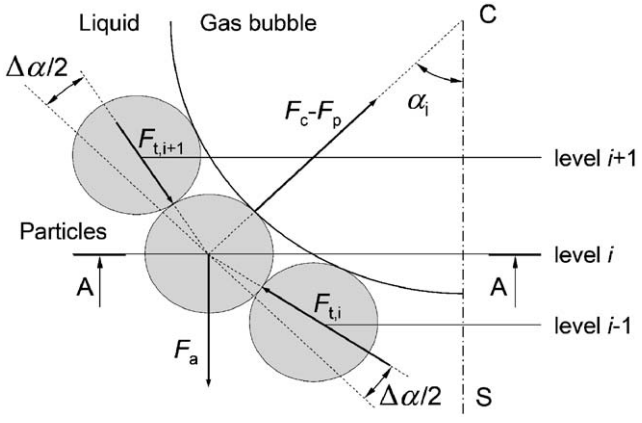

Fig. 5. Schematic representations of forces acting on particles adhering to a spherical gas bubble as monolayer. C is the centre of bubble, S is the symmetry axis, A–A is the horizontal plane containing only the particles at level i, $F_c - F_p$ is the attraction due to capillary force corrected with the effect of bubble pressure, F_a is apparent gravitational force, and $F_{t,j}$ are tangential forces with $j = \{i, i+1\}$.

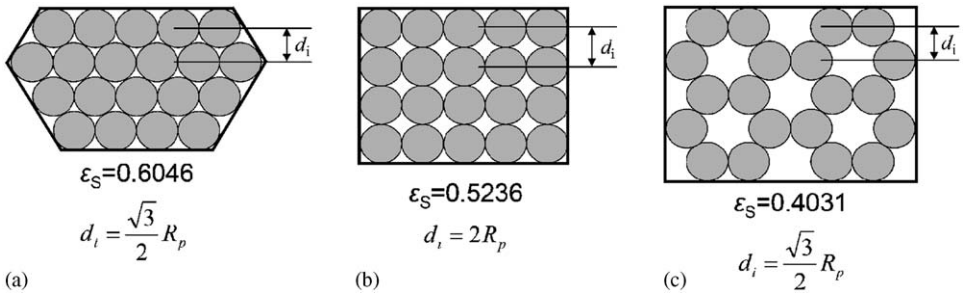

Fig. 6. Distribution of identical spheres as monolayer on a flat surface for high (a), medium (b), and low (c) volumetric fraction of solid ε_S. On real gas bubbles, the spherical particles cannot adopt such idealised distribution due to the surface curvature.

Table 1
Monolayer packing of spherical particles on a flat surface, according to Fig. 6

Case	(a)	(b)	(c)
Packing	Highest	Medium	Low
d_i	$\sqrt{3}R_p$	$2R_p$	$\sqrt{3}R_p$
ε_1	$\frac{\pi}{3\sqrt{3}}$	$\frac{\pi}{6}$	$\frac{\pi}{3\sqrt{3}}$
ε_2	1	1	$\frac{2}{3}$
$\varepsilon_S = \varepsilon_1\varepsilon_2$	0.6046	0.5236	0.4031

There is a single particle at level $i = 0$ and maximum $N_{i,\max}$ particles at level i. As these particles are placed on a circle, an approximate $N_{i,\max}$ value can be calculated as the ratio of this perimeter to the distance between two particles, except for zero level where only one particle is present:

$$N_{i,\max} = \begin{cases} \dfrac{2\pi(R_b + R_p)\sin\alpha_i}{2R_p}, & i > 0, \\ 1, & i = 0. \end{cases} \quad (16)$$

5.1. Particle packing in monolayer

The volume fraction ε_S of solid particles in the monolayer, depends on the particle packing. Vinke et al. (1991) described monolayer adhesion of particles to a gas bubble corresponding to a distance between two adjacent levels $d_i = 2R_p$ and a maximum number of particles at each level, $N_{i,\max}$. Van der Zon et al. (1999) incorporated the fraction of solid particle ε_S in the model as an additional parameter and present the results for $\varepsilon_S = 0.52$ corresponding to $d_i = 2R_p$.

Fig. 6 shows spherical particles regularly distributed on a planar surface, corresponding to high, medium and low packing. The particle packing depends on the distance between consecutive levels d_i in the range of $d_{i,\min} = \sqrt{3}R_p$ up to $d_{i,\max} = 2R_p$. Table 1 shows the corresponding values for the distances between consecutive rows and the particle packing for these cases. However, the product of the distance between consecutive levels d_i and the fraction of solid volume ε_S remains constant. Thus, the parameter ε_1 defines the density of particles as function of the distance between different levels:

$$\varepsilon_1 = \frac{\pi R_p}{3d_i}. \quad (17)$$

A level may contain a certain number of vacancies. Thus, the number of particles at level i contains only a fraction ε_2 of maximum number of particles defined by Eq. (16):

$$\varepsilon_2 = \frac{N_i}{N_{i,\max}}. \quad (18)$$

Both parameters ε_1 and ε_2 define the volumetric fraction of solid particles ε_S by a simple relation:

$$\varepsilon_S = \varepsilon_1\varepsilon_2. \quad (19)$$

5.2. Equilibrium forces on the lowest particle in monolayer

As in case of a single particle, the equilibrium is based on the forces: F_g, F_b, F_p and F_c. However, the particles on level $i+1$ force down the particles on level i and so on. The tangential force of a particle below level i will be denoted by $F_{t,i}$. Since action and reaction are equal and opposite, the sum of tangential forces $F_{t,i+1}$ of all N_{i+1} particles at level $i+1$ has as reaction the sum of tangential forces $F_{t,i}$ of all N_i particles at level i. Clearly, no tangential forces exist above the last level $i_{\max}$ because there are no particles. The tangential forces are increasing from a minimum value at the maximum level $i_{\max}$, to a maximum value at the level $i = 0$.

The detachment of a solid particle at level i depends on the sum of *radial forces*, perpendicular to the G–L interface. The relation between the radial and tangential forces is given by

$$F_{d,i} = F_a \cos\alpha_i - F_c + F_p + \frac{N_{i+1}F_{t,i+1} + N_i F_{t,i}}{N_i} \sin\frac{\Delta\alpha}{2} \quad \text{(radial)}. \quad (20)$$

One can imagine an iterative method to calculate *tangential forces* $F_{t,i}$ by starting with the level n downward to the level 0. The next equation acts as force balance for one

particle at level i on tangential direction to the bubble:

$$F_a \sin \alpha_i + \frac{N_{i+1}F_{t,i+1} - N_i F_{t,i}}{N_i} \cos \frac{\Delta\alpha}{2} = 0 \quad \text{(tangential)}. \tag{21}$$

From Eqs. (16), (18) and (21) one can calculate the sum of tangential forces of particles at level $i = 1, \ldots, i_{\max}$:

$$N_i F_{t,i} = \frac{\pi\varepsilon_2 F_a (R_p + R_b)}{R_p \cos \Delta\alpha/2} \sum_{k=i}^{i_{\max}} \sin^2 \alpha_k. \tag{22}$$

The detachment force for the particle at level $i=0$ is highest as consequence of summation of the tangential forces. For small particles and hence small $\Delta\alpha$ angle, $\cos(\Delta\alpha/2)$ can be approximated with 1.

At level $i = 0$ (bubble bottom) there is a single particle, $N_0 = 1$. The particles at the level $i = 1$ cannot come closer than a distance of $2R_p$. This value is independent on particle packing.

After replacement of $N_i F_{t,i}$ term from Eq. (22) in Eq. (20) and substitution of $\sin(\Delta\alpha/2)$ from Eqs. (14) and (17), the detachment force $F_{d,0}$ for $i = 0$ becomes

$$F_{d,0} = (F_a - F_c + F_p) + \pi\varepsilon_2 F_a \sum_{k=0}^{i_{\max}} \sin^2 \alpha_k. \tag{23}$$

The bubble is covered with a maximum number of particles at maximum coverage angle $\alpha_{\max}$ when $F_{d,0}$ is zero and $(F_a - F_c + F_p)$ term has a minimum value for maximum adhesion force $F_{\text{adh,max}}$. The last term containing the sum of the squared sinus is approximated by an integral and then integrated analytically, thus given

$$\begin{aligned} F_{\text{adh,max}} &= -\min(F_a - F_c + F_p) \\ &= \max\left(\pi\varepsilon_2 F_a \sum_{k=0}^{i_{\max}} \sin^2 \alpha_k\right) \\ &= \pi\varepsilon_2 F_a \frac{1}{\Delta\alpha} \int_0^{\alpha_{\max}} \sin^2 \alpha \, \mathrm{d}\alpha \\ &= \frac{3\varepsilon_S F_a (R_p + R_b)}{2R_p} (\alpha_{\max} - \sin \alpha_{\max} \cos \alpha_{\max}) \end{aligned} \tag{24}$$

Fig. 7 shows the maximum coverage angle $\alpha_{\max}$ as function of three-phase contact angle θ for different particle and bubble size. The maximum coverage angle $\alpha_{\max}$ was calculated according to Eq. (24). The maximum adhesion force $F_{\text{adh,max}}$ calculated with φ_{opt} from Eq. (7) or φ^*_{opt} from Eq. (8) gives almost the same results.

The coverage angle increases by increasing the contact angle θ, or by decreasing the particle size R_p. For small particles, the coverage angle increases by decreasing the bubble size. Small bubbles can be better covered by adhering particles than large bubbles. This fact is well known in flotation practice. For large particles, the effect of bubble pressure according to Eq. (3) is higher, resulting in lower adhesion force and lower coverage angles.

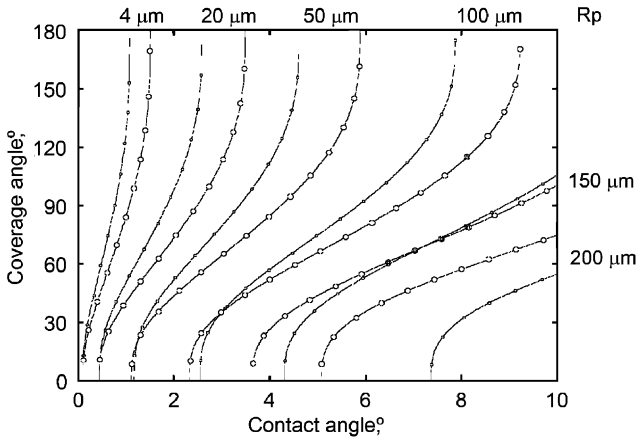

Fig. 7. Influence of three-phase contact angle θ on maximum bubble coverage angle $\alpha_{\max}$ for particle size in the range of R_p=4–200 μm, for small (o, R_b=0.25 mm) and large (O, R_b=0.5 mm) bubbles. Other parameters: ρ_L=998 kg m^{-3}, P_v=1 cm^3 g^{-1}, ρ_S=1374 kg m^{-3}, γ_{LG}=0.072 N m^{-1}.

By substitution of Eqs. (2), (9), (10) and (19) in Eq. (24), the following equation allows the estimation of maximum coverage angle $\alpha^*_{\max}$ of small spherical particles from three-phase contact angle:

$$\sin^2 \frac{\theta}{2} = \varepsilon_S \cdot \frac{(\rho_S - \rho_L) g R_p (R_p + R_b)}{\gamma_{LG}} \cdot (\alpha^*_{\max} - \sin \alpha^*_{\max} \cos \alpha^*_{\max}). \tag{25}$$

The left hand term is derived from the maximum adhesion force $F_{\text{adh,max}}$ of a spherical particle. A similar approach for a cylindrical particle shows that maximum adhesion force is proportional with $\sin \theta$. These two cases of spherical and cylindrical particles demonstrate that maximum adhesion force and the left hand term in Eq. (25) depend on the contact angle but also on the particle shape and orientation. Therefore, the influence of particle shape on maximum adhesion force can be described by a generic function $\Phi(\theta)$.

The right side of Eq. (25) contains the ratio of gravitational force to capillary force that may be attributed to a dimensionless number similar to the Eötvos or Bond number. This dimensionless number, referred as E_{pb}, includes the liquid and solid densities ρ_L and ρ_S, gravitational acceleration g, particle and bubble size R_p and R_b, and superficial tension of liquid γ_{LG}. The last factor in Eq. (25) contains a single variable, the bubble coverage angle. If the bubble is not perfect spherical, this expression can be represented by a generic function $f(\alpha_{\max})$. Thus, the equation describing the adhesion of a monolayer of particles to a gas bubble was generalised to nonspherical particles and bubbles as follows:

$$\Phi(\theta) = \varepsilon_S E_{pb} f(\alpha_{\max}). \tag{26}$$

The bubble coverage angle $\alpha_{\max}$ depends on the particle shape, orientation and surface roughness through function Φ, on the three-phase contact angle θ, on the volumetric fraction of solid particles in monolayer ε_S, on dimensionless E_{pb} number and on the bubble shape through the function f.

The total number of solid particles adhering to a bubble as a monolayer N_T can be related to maximum coverage angle $\alpha_{\max}$:

$$N_T = 3\varepsilon_S\left(1+\frac{R_b}{R_p}\right)^2(1-\cos\,\alpha_{\max}). \tag{27}$$

6. Multilayer adhesion

Let us consider an aggregate of particles adhering to a gas bubble through successive layers. The first layer of particles adheres directly to the gas bubble through adhesion forces. The cohesion forces between particles keep the subsequent layers together. Fig. 8 shows the forces acting on a single particle surrounded by other particles. Due to the symmetry axis S, only the tangential and radial forces in vertical cross-section are considered here.

As in the case of monolayer adhesion discussed before, the particles of each layer j are counted starting with $i=0$ on the symmetry axis to $i_{\max,j}$. Different layers may have different coverage angles. The first layer of particles $j=1$, adheres directly to gas bubble. The following layers $j=2,\ldots,j_{\max}$ are kept together by cohesion forces on radial direction. The distance between two consecutive layers defined as d_j is assumed to be constant. The particles forming the layer j are placed at the same distance from the bubble centre on the sphere of radius R_j as described below:

$$R_j = R_b + R_p + (j-1)d_j. \tag{28}$$

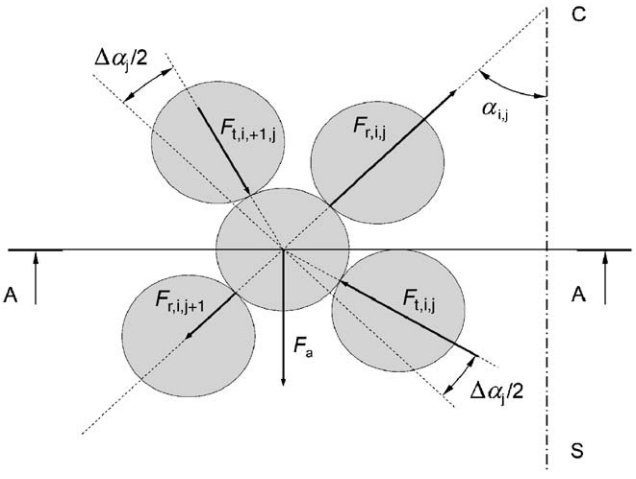

Fig. 8. Schematic representations of forces acting on particles adhering to a spherical gas bubble as multilayer. C is the bubble centre, S is the symmetry axis, A–A is an horizontal plane containing the particles of level i and layer j, F_a is apparent gravitational force, $F_{r,i,k}$ are radial forces responsible for the cohesion between particles with $k=\{j, j+1\}$, and $F_{t,k,j}$ are tangential forces between particles on the same layer with $k=\{i, i+1\}$.

Table 2
Multilayer packing of spherical particles on a flat surface without vacancies, $\varepsilon_2=1$

Case	(a)	(b)	(c)	(d)
Monolayer packing	Fig. 6(a)	Fig. 6(a)	Fig. 6(b)	Fig. 6(b)
ε_1	$\frac{\pi}{3\sqrt{3}}$	$\frac{\pi}{3\sqrt{3}}$	$\frac{\pi}{6}$	$\frac{\pi}{6}$
Distance between layers	Minimum	Maximum	Minimum	Maximum
d_j	$\frac{\sqrt{2}}{\sqrt{3}}2R_p$	$2R_p$	$\sqrt{2}R_p$	$2R_p$
ε_3	$\frac{\sqrt{3}}{\sqrt{2}}$	1	$\sqrt{2}$	1
$\varepsilon_S=\varepsilon_1\varepsilon_2\varepsilon_3$	0.7405	0.6046	0.7405	0.5236

The angle $\Delta\alpha_j$ is defined similar to $\Delta\alpha$ from Eq. (14), but now dependent on the layer position j:

$$\sin\frac{\Delta\alpha_j}{2}=\frac{d_i}{2R_j}. \tag{29}$$

The line connecting the centres of particle and bubble, and the symmetry axis S forms an angle $\alpha_{i,j}$ defined by

$$\alpha_{i,j}=i\Delta\alpha_j. \tag{30}$$

As in the case of monolayer adhesion, all particles at coordinates (i, j) are placed on a circle around of the symmetry axis and they form a level. The maximum number of particles $N_{i,j,\max}$ on this level can be calculated as below:

$$N_{i,j,\max}=\begin{cases}\dfrac{\pi R_j\,\sin\,\alpha_{i,j}}{R_p}, & i>0,\\ 1, & i=0.\end{cases} \tag{31}$$

6.1. Multilayer packing

The particles can be packed in each monolayer according to parameters ε_1 and ε_2. Successive monolayers are packed together as multilayer agglomerates. Thus, a new parameter ε_3 defines the layer packing of as function of the interlayer distance d_j. If the distance between two adjacent layers is maximal and equal to particle size $d_j=2R_p$, the volumetric fraction of solid ε_S is equal for the monolayer and multilayer. The calculation of particle packing for two minima and two maximum distances d_j, is shown in Table 2. The packing of consecutive layers can be defined as below:

$$\varepsilon_3=\frac{2R_p}{d_j}. \tag{32}$$

Hence, overall volumetric fraction of solid becomes:

$$\varepsilon_S=\varepsilon_1\varepsilon_2\varepsilon_3. \tag{33}$$

6.2. Cohesive forces in multiplayer adhesion

When a particle is suspended below other particle, the minimum cohesive force F_{coh} equals the apparent gravitational force F_a as can be shown in Fig. 9a. One particle can

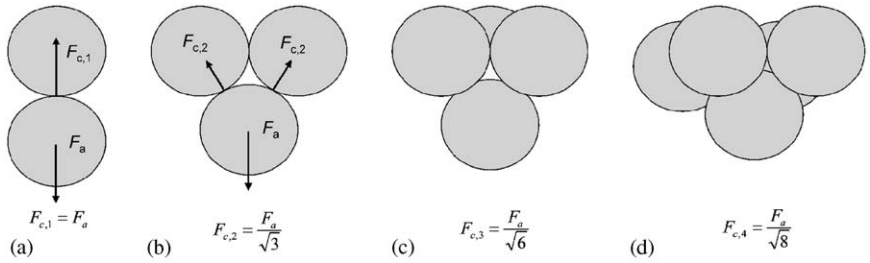

Fig. 9. Relation between the particle packing and aggregate cohesion strength. Increasing the number of bounded particles from 1 in (a) to 4 in (d) results in stronger cohesion forces, better particle packing and higher volumetric fraction of solid ε_S.

Table 3
Minimum cohesive force of a pendant particle attached to an upper layer through n equivalent particles as shown in Fig. 9

n	Required force, F_a	cos φ	Minimum cohesion force, F_{coh}
1	$F_{\text{coh}} \cos \varphi$	1	F_a
2	$2F_{\text{coh}} \cos \varphi$	$\frac{\sqrt{3}}{2}$	$\frac{F_a}{\sqrt{3}}$
3	$3F_{\text{coh}} \cos \varphi$	$\frac{\sqrt{2}}{\sqrt{3}}$	$\frac{F_a}{\sqrt{6}}$
4	$4F_{\text{coh}} \cos \varphi$	$\frac{\sqrt{2}}{2}$	$\frac{F_a}{\sqrt{8}}$

be suspended through n equivalent particles of a higher layer by a smaller force $F_{\text{coh},n}$, as presented in Table 3 and Fig. 9. Consequently, the distance d_j between the adhering particle and the previous layer decreases for higher values of n. Thus, a relationship exists between the particle packing and the cohesive force of one particle to the upper layer. We will further refer to the cohesion of a particle to a monolayer, not to the cohesion between two individual particles.

6.3. Equilibrium forces in multilayer

A single spherical particle is in equilibrium if the sum of forces on radial or tangential direction is equal with zero, described by two below:

$$F_a \sin \alpha_{i,j} + \frac{N_{i+1,j} F_{t,i+1,j} - N_{i,j} F_{t,i,j}}{N_{i,j}} \cos \frac{\Delta\alpha_j}{2} = 0 \quad \text{(tangential)}, \tag{34}$$

$$F_a \cos \alpha_{i,j} + \left(\frac{R_{j+1}}{R_j}\right)^2 F_{r,i,j+1} - F_{r,i,j} + \frac{N_{i+1,j} F_{t,i+1,j} + F_{t,i,j} N_{i,j}}{N_{i,j}} \sin \frac{\Delta\alpha_j}{2} = 0 \quad \text{(radial)}. \tag{35}$$

Eq. (34) is similar to the Eq. (21) applied to a monolayer. Eq. (35) differs from the Eq. (20) mainly because the particle–bubble attractive interaction $F_c - F_p$ is replaced by attractive cohesive forces between particles. The aggregate is stable if any radial force do not exceed the cohesion force, $F_{r,i,j} < F_{\text{coh,max}}$. Note that radial force in Eq. (35) varies from layer to layer according to a constant solid angle, proportional to R_j^2.

The tangential forces from Eq. (34) can be computed for each particle independent on radial forces, by iteration, starting with the maximum values of $i_{\max}$ as described below

$$F_{t,i,j} = \frac{F_a}{N_{i,j} \cos \Delta\alpha_j/2} \sum_{k=i}^{i_{j,\max}} (N_{k,j} \sin \alpha_{k,j}). \tag{36}$$

The radial forces from Eq. (35) depend on the tangential forces available now from Eq. (36). However, the radial forces of each layer are maximal for particles on the symmetry axis, as below:

$$F_{r,0,j} = \frac{\pi\varepsilon_2 F_a}{R_j^2} \sum_{k=j}^{j_{\max}} \left[R_k^2 \sum_{i=1}^{i_{\max,k}} \sin^2(\alpha_{i,k}) \right] + \frac{F_a}{R_j^2} \sum_{k=j}^{j_{\max}} R_k^2. \tag{37}$$

Overall aggregate stability depends on the radial forces of first two axi-symmetric particles suspended at the bottom of the bubble. The first particle at ($i = 0$, $j = 1$) is directly attached to the bubble. This particle is characterised by the highest particle–bubble adhesion force $F_{\text{adh,max}} = F_{r,0,1} - F_a$. The second particle at ($i = 0$, $j = 2$) adheres to the first monolayer. This particle is characterised by the highest cohesion force $F_{\text{coh,max}} = F_{r,0,2}$. Eq. (37) can be applied when the shape of particle agglomerate is available from microscopic images. The particle distribution—in terms of the number of layers $j_{\max}$ and the coverage angles of each monolayer $\alpha_{\max,j}$—can be estimated by maximising the total number of particles. Thus, it becomes possible: (i) to calculate the adhesion and cohesion forces from the agglomerate structure, or (ii) to estimate the most probable configuration of particles adhering to a gas bubble when the forces are known. The second case allows the calculation of bubble coverage angle of first monolayer, $\alpha_{\max,1}$.

6.4. Multilayer with constant thickness

If the thickness of particles h_T and the coverage angle $\alpha_{i,j} = \alpha_{\max}$ are constants, the previous equation leads by the

summation of all layers k and by integration of all levels i to:

$$F_{r,0,j} = \frac{3\varepsilon_S F_a R_j h_j}{2R_p^2} f(\alpha_{\max}) \left(1 + \frac{\delta_j}{2}\right) \left(1 + \delta_j + \frac{\delta_j^2}{2}\right) + \frac{\varepsilon_3 F_a h_j}{2R_p} \left(1 + \delta_j + \frac{\delta_j^2}{3}\right), \quad (38)$$

where the function f has been already introduced by Eq. (26). The term δ_j resulting by integration of Eq. (37) is defined as below:

$$\delta_j = \frac{h_j}{R_b + R_p + (j-1)d_j}, \quad (39)$$

where h_j is the thickness of particle aggregate below of layer j, and h_T is total thickness of all layers.

$$h_j = h_T - R_p - (j-1)d_j. \quad (40)$$

Eq. (40) allows the calculation of maximum adhesion force $F_{\text{adh,max}}$ for $j = 1$ and maximum cohesion force $F_{\text{coh,max}}$ for $j = 2$. The radial forces becomes proportional with the number of layers for $\alpha_{\max} > 20°$ and $R_b > 20R_p$. In this case, the forces are

$$F_{\text{adh,max}} = \frac{3\varepsilon_S F_a (R_b + R_p)(h_T - R_p)}{2R_p^2} f(\alpha_{\max}) + \frac{\varepsilon_3 F_a (h_T - R_p)}{2R_p} - F_a, \quad (41)$$

$$F_{\text{coh,max}} = F_{\text{adh,max}} - \frac{3\varepsilon_1\varepsilon_2 F_a (R_b + R_p)}{R_p} f(\alpha_{\max}). \quad (42)$$

These latter equations allow the calculation of maximum coverage angle $\alpha_{\max}$ and agglomerate thickness h_T from maximum adhesion and cohesion forces, or the other way around. The thickness h_T depends on the cohesion forces $F_{\text{coh,max}}$. At low cohesion forces, the particles may adhere to a bubble only as a monolayer. At higher cohesive forces two or more layers can adhere to the bubble, but the coverage angle is decreasing. Very high cohesive forces between particles increase the aggregate thickness and decrease the coverage angle. In this case, the aggregate can be detached from the gas bubble as a whole. Thus, an aggregate of particles has the same properties as a single but bigger particle, with a lower solid density.

6.5. Number of particles in multilayer

In the general case, the total number of particles N_T adhering to a bubble in the form of a multilayer can be calculated by summation of all levels of all layers:

$$N_T = \sum_{j=1}^{j_{\max}} \sum_{i=0}^{i_{\max,j}} N_{i,j}. \quad (43)$$

In particular, if the thickness of particles h_T and the coverage angle $\alpha_{\max}$ are constants, the total weight of particles adhering to a gas bubble is $W_T = N_T W_0$, where the number of particles N_T is given by

$$N_T = \frac{\varepsilon_S \int_0^{2\pi} \int_{R_b}^{R_b+h_T} r^2 \int_0^{\alpha_{\max}} \sin\alpha \, d\alpha \, dr \, d\beta}{4\pi R_p^3/3} \approx 3\varepsilon_S \frac{R_b(R_b + h_T)h_T}{2R_p^3}(1 - \cos\alpha_{\max}). \quad (44)$$

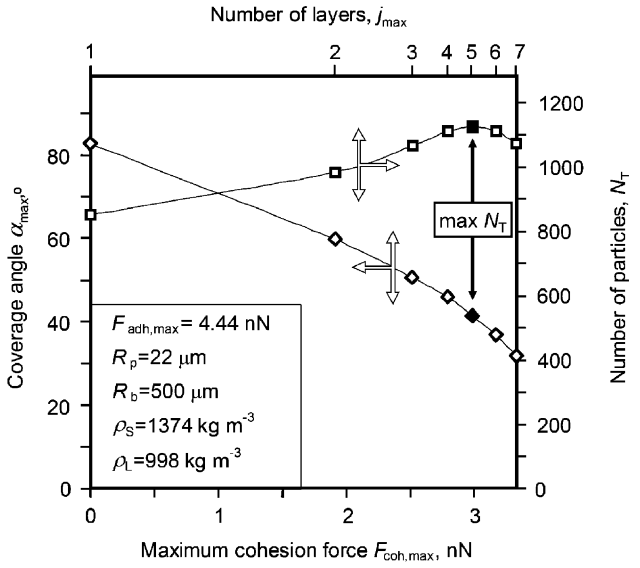

Fig. 10. Influence of maximum cohesion force on number of layers, bubble coverage angle (◇), and number of particles adhering to a gas bubble (□).

Fig. 10 shows the influence of cohesion forces on the multilayer configuration as bubble coverage angle, number of layers and total number of particles. In the case of one layer, the coverage angle was calculated from maximum adhesion force, using Eq. (23) or (37). Consequently, the number of particles results from Eq. (43). For more than one layer, the maximum number of particles N_T was determined by optimisation, varying the number of layers and particles on each layer. There is one equality constraint given by a constant adhesion force and inequality constraints given by the coverage angle of each layer, $\alpha_{\max,1} \geqslant \alpha_{\max,2} \geqslant \cdots \geqslant \alpha_{\max,j\,\max}$. The cohesion forces result from Eq. (37), where $F_{\text{coh,max}} = F_{r,0,2}$.

Fig. 10 shows the maximum bubble coverage of 82° at zero cohesion forces, corresponding to a monolayer of particles. The cohesive force decreases the coverage angle but increases the number of layers. Note that the number of layers was represented on a secondary axis but on the same coordinate as the cohesion force.

The second curve in Fig. 10 shows the total number of particles in aggregate. Up to five layers, the cohesion force increases the number of particles. The maximum number of particles shown in the figure (max $N_T = 1123$) occurs at $F_{\text{coh,max}} = 2.98$ nN. The coverage angle is about half of the monolayer coverage angle. Beyond this maximum, the

coverage angle and the maximum number of particles are decreasing.

7. Conclusions

The adhesion of small particles to gas bubbles under stagnant conditions was described by a generalised model. The model correlates the maximum particle–bubble adhesion force and the intraparticle cohesive forces to the bubble coverage angle and aggregate thickness, explaining mono- and multilayer adhesion. For known geometries e.g. spherical particles with smooth, homogeneous and clean surfaces, the maximum adhesion force can be directly computed from three-phase contact angle. However, the use of the maximum adhesion force instead of the three-phase contact angle reduces the number of model parameters and extends the model applicability to porous particles.

Particles adhere to gas bubbles as a monolayer only when the particle–particle cohesion forces are negligible as compared to the apparent weight of a single particle immersed in the liquid. When this is not the case, particles may adhere as an aggregate or multilayer. Higher adhesive forces result in higher bubble coverage with particles and higher number of particles adhering to a bubble. An increase in the cohesion forces between particles results in higher aggregate thickness but lower bubble coverage. If the cohesion forces exceed the adhesion forces, the particles may form large aggregates, unable to adhere to gas bubbles due to their apparent weight.

The model developed in this work also explains the influence of agglomeration on the gas-liquid mass transfer in slurry bubble reactors. Thus, an increase of the intra-particle cohesive forces produces the particle agglomeration, resulting in lower bubble coverage and lower gas-liquid mass transfer, in agreement with the conclusion of Vinke et al. (1991b) and the experiments of van der Zon et al. (1999).

Notation

d_i distance between any two adjacent levels, m
d_j distance between any two adjacent layers, m
E_{pb} dimensionless Eotvos number for particle–bubble interactions, $(\rho_S - \rho_L) g R_p (R_p + R_b)/\gamma_{LG}$
f function characteristic to bubble shape; $f(x) = x - \sin(x)\cos(x)$ for spherical bubbles
F_a apparent weight of a particle in liquid, N
F_{adh} adhesion force of a particle to a gas bubble, N
F_b buoyancy force of a particle in liquid, N
F_c capillary force of a particle attached to a bubble, N
F_d detachment force defined by Eq. (6), N
F_g gravity force of a particle having the pores filled with liquid, N
F_p force resulting from the capillary pressure in the bubble, N
$F_{r,i,j}$ radial forces in mono- (absent if $j = 1$ is unique) and multi-layer adhesion, N
$F_{t,i,j}$ tangential forces in mono- (absent if $j = 1$ is unique) and multi-layer adhesion, N
g gravitation constant equal to 9.807, $\mathrm{m\,s^{-2}}$
h_j thickness of particle aggregate below of the centre of a particle of layer j, m
h_T thickness of particle aggregate in multilayer adhesion, m
i level position in a monolayer (see Fig. 5)
j layer position in an aggregate
N number of particles in a cluster, except the particle adhering to bubble
R radius, m

Greek letters

α coverage angle defined as the angle formed by the centre of a particle, the centre of a spherical bubble, and the lowest pole of the bubble (see Figs. 5 and 8), rad
γ_{LG} superficial tension of G–L interface, $\mathrm{N\,m^{-1}}$
δ_j ratio of the thickness h_j to the radius R_j corresponding to a particle on layer j
$\Delta\alpha$ angle formed by the centre of a spherical bubble and two consecutive levels, in vertical plane, rad
ΔP difference in pressure of gas and liquid at the three-phase contact line, $P_G - P_L$, Pa
Δz position of three-phase contact line of an adhering particle relative to free liquid meniscus, m
ε_1 volumetric fraction of spherical particles in a monolayer
ε_2 factor accounting for the presence of voids
ε_3 factor accounting for the interlacement of consecutive layers
ε_S volumetric fraction of solid particles in monolayer or multilayer aggregate
θ three-phase contact angle for a single particle adhering at the G–L interface, rad
ρ_L liquid density, $\mathrm{kg\,m^{-3}}$
ρ_S density of particles having the pores filled with liquid, $\mathrm{kg\,m^{-3}}$
φ angle of penetration of a particle into the G–L interface, rad
Φ function characteristic to particle shape, orientation, roughness and/or porosity

Superscripts

$*$ approximated by a shortcut method
N number of particles
s solid particle, pores filled with liquid

Subscripts

adh adhesion of particle to gas bubble
b bubble

coh	cohesion between particles
i	*i*th level of the layer
j	*j*th layer in multilayer adhesion
max	maximum value
min	minimum value
opt	optimum value, minimum or maximum
p	particle
r	radial
t	tangential

Acknowledgements

This research is supported by the Technology Foundation STW, applied science division of NWO and the technology program of the Ministry of Economic Affairs. The authors also gratefully acknowledge Akzo-Nobel, DSM Research B.V., Shell Global Solutions, Engelhard B.V., Promeks ASA, Norit B.V. and Sasol for their financial support.

References

Alper, E., Öztürk, S., 1986. Effect of fine solid particles on gas–liquid mass transfer rate in a slurry reactor. Chemical Engineering Communications 46, 147–158.

Alper, E., Wichtendahl, B., Deckwer, W.D., 1980. Gas absorption mechanism in catalytic slurry reactors. Chemical Engineering Science 35, 217–222.

Beenackers, A.A.C.M., van Swaaij, W.P.M., 1993. Mass transfer in gas–liquid slurry reactors. Chemical Engineering Science 48, 3109–3139.

Chibowski, E., Perea-Carpio, R., 2002. Problems of contact angle and solid surface free energy determination. Advances in Colloid and Interface Science 98, 245–264.

Dagaonkar, M.V., Heeres, H.J., Beenackers, A.A.C.M., Pangarkar, V.G., 2003. The application of fine TiO_2 particles for enhanced gas absorption. Chemical Engineering Journal 92, 151–159.

Dietrich, E., Mathieu, C., Delmas, H., Jenck, J., 1992. Raney-nickel catalysed hydrogenations: gas–liquid mass transfer in gas-induced stirred slurry reactors. Chemical Engineering Science 47 (13/14), 3597–3604.

Fielden, M.L., Hayes, R.A., Ralston, J., 1996. Surface and capillary forces affecting air bubble–particle interactions in aqueous electrolyte. Langmuir 12, 3721–3727.

Joly-Vuillemin, C., De Bellefon, C., Delmas, H., 1996. Solid effects on gas–liquid mass transfer in three-phase slurry catalytic hydrogenation of adiponitrile over Raney nickel. Chemical Engineering Science 51, 2149–2158.

Lavelle, K., McMonagle, J.B., 2001. Mass transfer effects in the oxidation of aqueous organic compounds over a hydrophobic solid catalyst. Chemical Engineering Science 56, 5091–5102.

Lee, Y.Y., Tsao, G.T., 1972. Oxygen absorption into glucose solution. Chemical Engineering Science 27, 1601–1608.

Lindner, D., Werner, M., Schumpe, A., 1988. Hydrogen transfer in slurries of carbon supported catalysts (HPO process). A.I.Ch.E. Journal 34 (10), 1691–1697.

Malandrini, H., Clauss, F., Partyka, S., Douillard, J.M., 1997. Interactions between talc particles and water and organic solvents. Journal of Colloid and Interface Science 194, 183–193.

Ortiz-Arroyo, A., Larachi, F., Iliuta, I., 2003. Method for inferring contact angle and for correlating static liquid hold-up in packed beds. Chemical Engineering Science 58, 2835–2855.

Preuss, M., Butt, H.-J., 1998. Direct measurement of particle–bubble interactions in aqueous electrolyte: dependence on surfactant. Langmuir 14, 3164–3174.

Shultze, H.J., 1984. Physico-chemical elementary processes in flotation. Developments in Mineral Processing, vol. 4, Elsevier Science, New York.

Tinge, J.T., Drinkenburg, A.A.H., 1992. Absorption of gases into activated carbon–water slurries in a stirred cell. Chemical Engineering Science 47 (6), 1337–1345.

Tinge, J.T., Drinkenburg, A.A.H., 1995. The enhancement of the physical absorption of gases in aqueous activated carbon slurries. Chemical Engineering Science 50 (6), 937–942.

Vinke, H., Hamersma, P.J., Fortuin, J.M.H., 1991a. Particle-to-bubble adhesion in gas/liquid/solid slurries. A.I.Ch.E. Journal 37, 1801–1809.

Vinke, H., Bierman, G., Hamersma, P.J., Fortuin, J.M.H., 1991b. Adhesion of small particles to gas bubbles: determination of small effective solid–liquid–gas contact angles. Chemical Engineering Science 46, 2497–2506.

Vinke, H., Hamersma, P.J., Fortuin, J.M.H., 1992. The enhancement of the gas-absorption rate in agitated slurry reactors due to the adhesion of gas-adsorbing particles to gas bubbles. Chemical Engineering Science 47 (13/14), 3589–3596.

Vinke, H., Hamersma, P.J., Fortuin, J.M.H., 1993. Enhancement of the gas-absorption rate in agitated slurry reactors by gas-adsorbing particles adhering to gas bubbles. Chemical Engineering Science 48 (12), 2197–2210.

Wimmers, O.J., Fortuin, J.M.H., 1988. The use of adhesion of catalyst particles to gas bubbles to achieve enhancement of gas adsorption in slurry reactors II. Determination of the enhancement in a bubble-containing slurry reactor. Chemical Engineering Science 43, 313–319.

Yan, N., Maham, Y., Masliyah, J.H., Gray, M.R., Mather, A.E., 2000. Measurement of contact angles for fumed silica nanospheres using enthalpy of immersion data. Journal of Colloid and Interface Science 228, 1–6.

van der Zon, M., Hamersma, P.J., Poels, E.K., Bliek, A., 1999. Gas–solid adhesion and solid–solid agglomeration of carbon supported catalysts in three phase slurry reactors. Catalysis Today 48, 131–138.

van der Zon, M., Thoolen, H., Hamersma, P.J., Poels, E.K., Bliek, A., 2001. Agglomeration and adhesion of catalyst particles in gas–liquid reactors. Catalysis Today 66, 263–270.